SYNTHESIS AND CHARACTERIZATION OF THIOPHENE BASED METAL FREE DYE SENSITIZERS FOR SOLAR CELLS, THEIR PHOTO-RESPONSE AND CHEMOSENSING PROPERTIES

A MINI THESIS SUBMITTED IN PARTIAL FULFILMENT

OF THE REQUIREMENTS FOR THE DEGREE OF

MASTER OF SCIENCE IN CHEMISTRY

OF

THE UNIVERSITY OF NAMIBIA

BY

INGRID PANDULENI SHIKANGALA

201070316

April 2020

Supervisor: Prof. V. Uahengo (Department of Chemistry and Biochemistry, University of Namibia)

ABSTRACT

In 1991, Michael Grätzel and co-workers developed a new photovoltaic cell known as Dye Sensitized solar cells (DSSCs); these photovoltaic semiconductor devices convert solar radiation directly into electricity [1]. Metal-free sensitizers such as organic dyes and natural dyes have received attention as alternative DSSC applications and have been extensively developed [2]. Two metal free dyes were reported. These dyes were prepared through Schiff base synthetic methods, which are easy to follow.

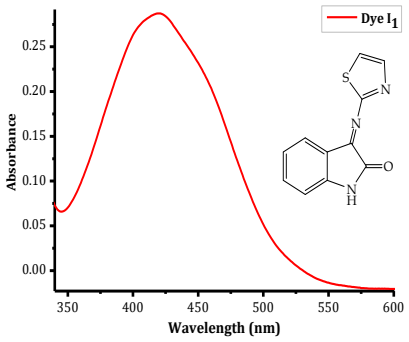

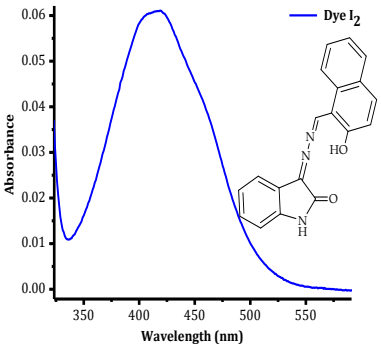

The dyes absorb light in the visible light region. The interaction with ionic other species (sensing) properties were studied, with dye I1 (**sensor A**) and dye I2 (**sensor B**) designations. These recognition properties towards various ions were investigated firstly by naked eye observation and secondly by spectroscopic methods such as UV-vis in water-soluble DMSO. As a result, the addition of mercury (Hg^{2+}) to **sensor A** displayed a clearly visible “naked eye” detectable colorimetric activities (from yellow to pale yellow), while the addition of fluoride (F^-) and cyanide (CN^-) to **sensor B** also displayed "naked eye" detectable colorimetric activities (from pink to purple), in DMSO at ambient temperature. Thus each dye possesses a duality function, as an

organic DSSC as well as a colorimetric sensors for discriminating specific ionic species in a given environment.

TABLE OF CONTENTS

LIST OF TABLES

LIST OF SCHEMES

LIST OF FIGURES

LIST OF ABBREVIATIONS AND/OR ACRONYMS

DSSCs	Dye Sensitized Solar Cells
PV	Photo voltaic
PCE	Photo current efficiency
TCO	Transparent conducting oxide
DMSO	Dimethylsulphoxide
DCM	Dichloromethane
THF	Tetrahydrofuran
EtOH	Ethanol
MeOH	Methanol
TBA	Tetrabutylammonium
FT-IR	Fourier Transform-Infrared Spectroscopy
eV	Electron volts
nm	Nanometers
HOMO	Highest Occupied Molecular Orbital
LUMO	Lowest Unoccupied Molecular Orbital
TiO_2	Titanium dioxide/Titania
PCE	Power conversion efficiency
VB	Valence band
CB	Conduction band

E_{HL}	HOMO–LUMO energy gap
^{1}H-NMR	proton Nuclear Magnetic Resonance
UV spectroscopy	Ultraviolet spectroscopy
ICT	Intra Molecular charge transfer
ppm	Parts per million
s	singlet
d	doublet
t	triplet
m	multiplets

ACKNOWLEDGEMENTS

I would like to glorify the almighty God for giving me wisdom as well as for his divine protection and guidance. I offer my deepest gratitude and special affection to my supervisor Prof Veikko Uahengo for guiding me throughout this interesting research topic, his generous advice, devoted assistance, encouragement in all stages of the work which were necessary for the progress of the research.

I would like to express greatest thanks to my dearest mother Loide Joolokeni Shinedima Shikangala for invaluable understanding, the support and the encouragement she offered during the work. I would also like to thank especially the fantastic people in the laboratory for the pleasant working environment and their helping hand in practical problems.

I am grateful to the National Commission on Research Science and Technology (NCRST) for sponsoring me to join the school of postgraduate studies. I appreciate the Chemistry and Biochemistry department at the University of Namibia (UNAM), and staff members for their sincere cooperation during my study.

I would like to express my sincere thanks to Mr Johannes H. Naimhwaka, who gave me fruitful suggestion during the whole work, as well as Paulina T. Endjala and Loini M. Kalipi who have been supporting me throughout the course of my studies.

DEDICATION

I wholeheartedly dedicate this mini-thesis to my beloved Family. Thank you for your never-ending support and for believing in me.

DECLARATIONS

I, Ingrid Panduleni Shikangala, hereby declare that this study is my own work and is a true reflection of my research and that this work or any part thereof has not been submitted for a degree at any other institution.

…… …… ……..……

Name of Student **Signature** **Date**

CHAPTER 1: INTRODUCTION

1.1 Background of the study

Owing to the increase in the world's population and technological development, the demand for fossil fuels has similarly been increasing. Therefore, the energy demand is proportional to the increase in the world's population, as forecasted by the international energy outlook of 2018, that the energy demand will increase by 28% between the year 2015 to 2040 [3]. Current research has been focused on finding a reliable, clean and equitable substitute for finite energy resources.

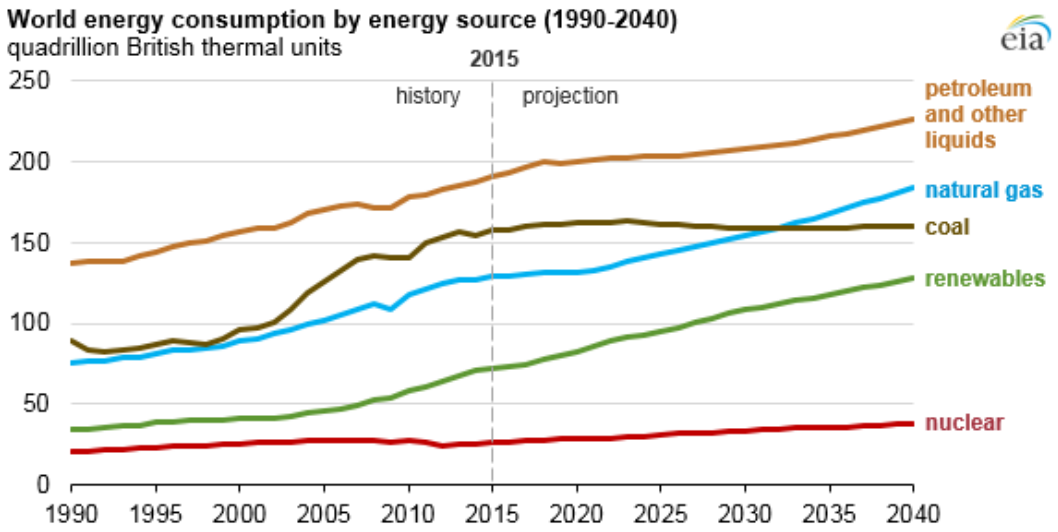

Figure 1. The world energy demand [3]

Owing to declining conventional non-renewable sources (coal, petroleum), research efforts are currently directed towards this area with the aim to find possible alternatives to substitute for the declining fossil fuels. This could be achieved by switching to renewable resources such as wind power, hydropower and or solar energy. Therefore harvesting solar energy from the sun would alternatively be a suitable solution, to account for this problem. In addition, solar cell technology that will harvest this solar energy should be developed. Moreover, these solar cells are expected to be reliable, efficient and cost-effective to compete with conventional sources [4]. A solar cell is

defined as a photonic device that converts photons with specific wavelengths directly into electricity [5].

Consequently, the way forward to overcome this energy problem is by utilising solar energy through the use of solar cells. However, over the past years, solar cells have gone through significant development [7]. These solar cells are further divided into generations: the first generation photovoltaic (PV) cells which are the most developed set of solar PV cells and are currently dominating the market, an example is single-crystalline (sc-Si) and multi-crystalline (mc-Si). However, this first generation solar cells are very expensive to produce and are associated with low efficiency [8]. The second-generation PV systems which are in their early stages of development, these cells are slowly growing and occupying the markets. However the second generation has lower efficiency compared to the first generation, even though their production costs are lower [8]. The third generation PV systems consist of technologies, such as concentrating PV (CPV) and organic PV cells that are still in the developing stage, as they have not yet been extensively commercialised. These solar cells are the most attention-grabbing in terms of low manufacturing costs. The dye sensitized solar cells (DSSCs) are also considered to be part of the third generation cells [7]. In comparison to silicon-based solar cells, the third generation solar cells are accompanied by the advantage of staying functional even under diffuse light.

In 1991, Michael Grätzel developed a new photovoltaic cell known as Dye Sensitized solar cells (DSSCs), these photovoltaic semiconductor devices convert solar radiation directly into electricity [1]. Dye-sensitized solar cells (DSSCs) have attracted research interest owing to their capabilities to convert solar light to electricity at low cost, ease of fabrication, can have different colour, and environmentally friendly as compared to other conventional photovoltaic devices [9]. At the moment the conversion efficiency

for the dye-sensitized solar cell is lower, but these types of DSSCs are forecasted as having the potential to produce higher efficiency in the future [5]. Subsequently, researchers are working with a focus on improving and understanding this technology better in order to develop DSSCs with higher conversion efficiency. There has been major progress in the DSSCs research fields having achieved a high conversion efficiency of up to 11% based on ruthenium dye, 12% based on porphyrin dye [7] and 10.1 % based on organic dye [10].

1.1.1 Characteristics of a good sensitizer

In order to improve the photovoltaic performance of DSSCs, the ultimate sensitizers should meet the following requirements [11-14]:

A sensitizer should possess certain unique characteristics such as a strong absorption in the visible range [11-14], high stability in its oxidized, ground, and excited states; suitable redox potential; good efficiency in the charge injection and regeneration processes [15], the most significant characteristic of the dye is its ability in absorbing the visible light spectrum from red to blue (as shown in figure 2) so that it can sensitize the wide band gap semiconductor material. [16].

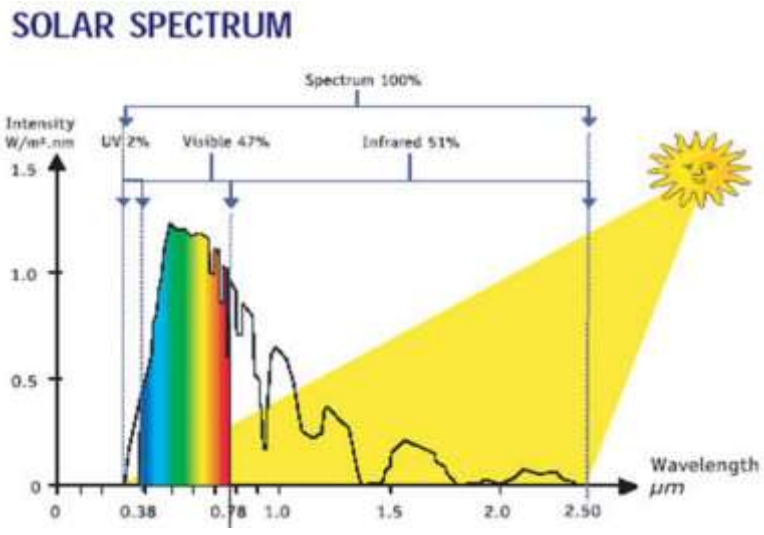

Figure 2. The solar spectrum [16]

1.2 Statement of the problem

Thiophene-based metal free dye sensitizers have a potential of increased photon harvesting. Their efficiency can be significantly improved if more research is focused on manipulating their molecular structures to optimize their photon harvesting properties at functional wavelengths. Generally, their synthetic methods are environmentally friendly, cost effective and from readily available materials. Thus, there is a great need to conduct research to improve the efficiency of these dyes, and hence to contribute towards finding a solution to the high energy demands in societies today.

1.3 Objectives of the study

The objectives of this study are:

(a) To design thiophene-based metal free dye sensitizers for solar cells

(b) To synthesize and characterize the thiophene-based metal free dye sensitizers

(c) To investigate the solvatochromic effect of the dyes towards their photo-responses in the visible region

(d) To investigate their chemosensing properties in aqueous-soluble solvents.

1.4 Significance of the study

Thiophene-based dye sensitizers have the efficiency of about 11%, thus more research is highly recommended to increase their efficiency for enhanced photon harvesting. In addition, electricity demand is increasing in Namibia, internationally high oil and commodity prices have had a current effect on the price of gas and coal. Yet there are opportunities such as harvesting solar energy since Namibia receive enough sunlight, solar energy is observed as one of the most ideal solutions to this, because of its abundant supply and inherent inexhaustibility.

1.5 Limitation of the study

This study will not construct the solar cell.

1.6 Delimitation of the study

This study will only focus on synthesizing and characterizing thiophene-based metal free dyes for DSSCs, their photo-response properties in the visible region, as well as their chemosensing properties.

CHAPTER 2: LITERATURE REVIEW

In this scenario, sunlight is utilised to produce electricity through the dye-sensitized solar cells (DSSCs), which has become the key solution to meet the energy demands. The dye molecule in DSSCs is responsible for harvesting the solar light and injection of electrons into the conduction band of the semiconductor [9]. In recent years, high conversion efficiencies of the DSSCs over 11% based on zinc-porphyrin and polypyridyl complexes of ruthenium have been achieved. However, the metal complexes application in DSSCs was limited by their toxicity, high cost, and synthesis difficult. In 2015, the best power conversion efficiency (PCE, η) of 13.1% have been attained for the DSSC based on a pure organic dye and is comparable to the metal-complex sensitizers [17].

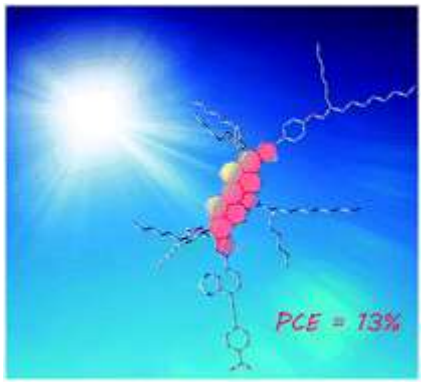

Figure 3: The Dithienopicenocarbazole dye with the PCE of 13% [17]

DSSCs are photovoltaic semiconductor devices that convert solar radiation directly into electricity. These DSSCs are further divided into five components which are as follows: (a). a conductive mechanical support, (b). a semiconductor film, (c). a sensitizer, (d). a redox couple (electrolyte), and (e). a counter electrode. Careful tuning of any of those two or three components above will end up in a DSSCs with increased efficiencies [18]. When the dye is exposed to light, it interacts with photons and goes to an excited state, which is sufficiently energetic to inject an electron into the TiO_2

conduction band. Therefore the electrons from the excited state of the dye enter the conduction band of TiO_2. The electrons then flow through the nanostructured porous TiO_2 to the transparent conducting oxide (TCO). This electron flow (or their kinetic energy) depends on the incident intensity of the light [7].

The DSSC operates as outlined in figure 3. [19, 20]. In the first step, photon is absorbed by the sensitizer that governs the promotion of an electron in the excited state. In the second step, an electron is injected from the excited state into the conduction band of the semiconductor and thereby leaving the sensitizer in its oxidised state. In step three the injected electron penetrates through the mesoporous structure of the semiconductor, this process driven by a chemical diffusion gradient and these electrons are collected at the transparent conductive electrode and then transferred to the external circuit. The fourth step shows that when the electron goes through the external circuit it reaches the counter electrode, where it interacts with the redox mediator turning it in its redox form. In the fifth step, the reduced state of the redox mediator finally reduces the oxidized sensitizer, in thereby regenerating the original dye and completing the circuit.

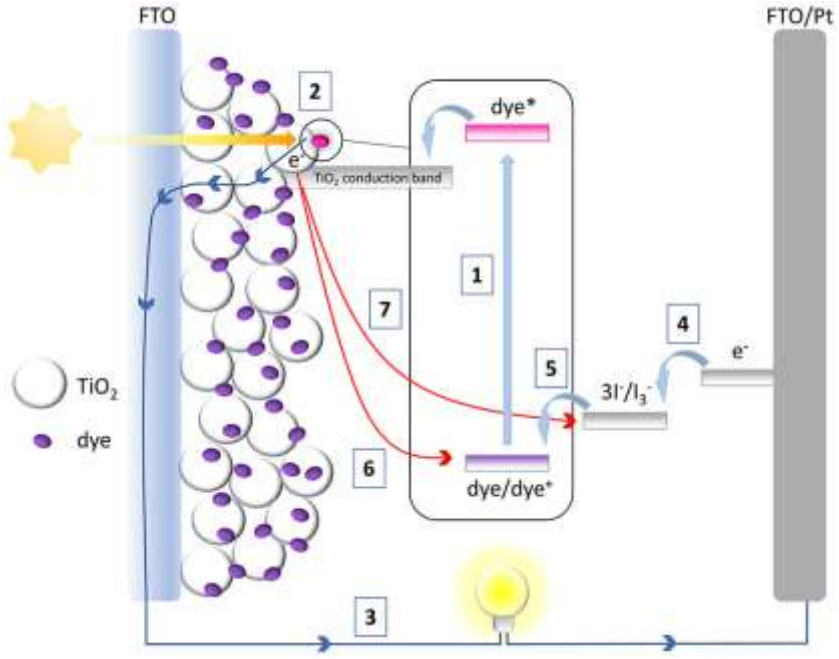

Figure 4. The Architecture and working principle of a typical DSSC [19]

Research efforts should be focused on improving photon absorption and charge injection into the conduction band. This can be achieved by manipulating the dyes' molecular structure thereby tuning its electronic and optical properties, which either increases the degree of absorption of incident photons within the functional wavelength or extend the functional range within the near-infrared range [21].

The HOMO-LUMO gap which defined as the energy difference between the highest occupied molecular orbital and the lowest unoccupied molecular orbital and it's an essential characteristic for analysing the performance of a dye-sensitized solar cell [22]. The energy of the HOMO-LUMO gap can tell us about what wavelengths the compound can absorb.

The HOMO–LUMO energy gap (E_{HL}) of the dyes will be estimated by the intersection point between its normalized absorption and emission spectra and it will be calculated from the equation: $E_{HL}/eV=1240/(\lambda\ /nm)=2.27$ eV [23].

Owing to a unique combination of efficient electron transfer, a moderate HOMO-LUMO gap, environmental stability, and structural versatility, thiophene-based π-conjugated systems have progressively supplanted other classes of systems [24].

Xiao et al [25] studied the effect of substituting the position of photo electronic properties of indolo[3,2-b]carbazole-based metal-free organic dyes. These dyes showed intensive absorption spectra in the wavelength of 300–600 nm and a narrow band gap of 2.29 eV, this means that these dyes absorbed visible light and they are suitable for use in solar cells. Their best power conversion efficiency (PCE) of 6.34% is obtained by the dye D2 due to its wider absorption spectra and strong steric hindrance, which can effectively suppress the undesirable dye aggregation [25].

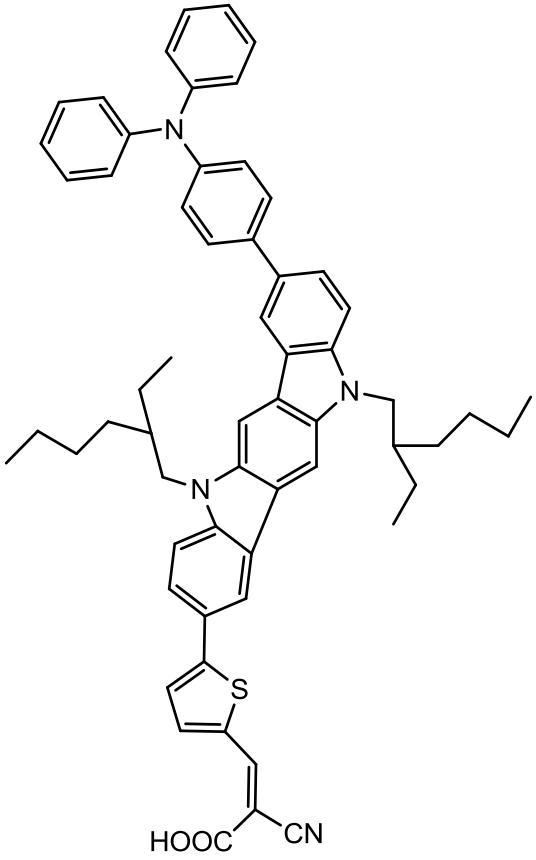

Figure 5. Structure of D2 [25]

An organic dye sensitizer primarily consists of three units with the D-π-A configuration (the donor-pi-acceptor configuration), the donor part is hydrophobic electron rich, while the acceptor is hydrophilic electron deficient and it acts as the anchoring site on the TiO_2 photoanode [26]. Moreover, each unit in the configuration has an influence on the overall efficiency of the cell, thus far, the modification of π-spacer is more important because it can tune the absorption region as well as allow the injection of the excited electrons into the conduction band of TiO_2 semiconductor [26]. The spectral features of D-π-A dyes are associated with the intramolecular charge transfer (ICT) from the donor to the acceptor and which is helpful for the electron injection into the conduction band of TiO_2 semiconductor anode [9, 27-30]. The best moieties for the π-conjugated bridge very frequently contain thiophene units, such as oligothiophenes, thienylenevinylenes, or dithienothiophene because of their excellent charge-transport properties, or phenylenevinylene [24]. The variation on the acceptor side is rather small, and in most cases, a cyanoacrylic acid group is used, with the anchoring carboxylic acid group elegantly incorporated into the acceptor moiety.

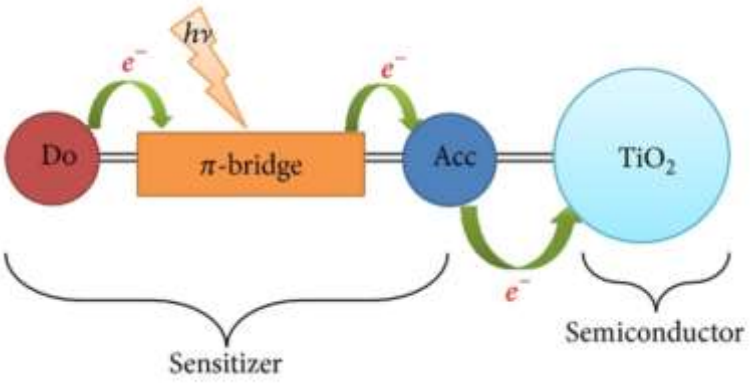

Figure 6. Design principle of an organic dye for TiO_2 photoanodes in DSSCs [31].

Hosseinzadeh et al [26] investigated the relationship between the structure and performance. The modification of the thiophene group near the donor group in dye T-BT has been done. It has been shown that the existence of the electron-rich pi spacer group is beneficial to enhance the intramolecular charge transfer (ICT) process owing to their ability to reduce the energy gap of the organic dye sensitizers, and consequently capturing more sunlight.

Three new 2D-π-A dyes (TK4, TK5 and TK6), composed of diarylamine donor groups, a dibenzofulvenethiophene core as the π-bridge, and a cyanoacrylic acid anchoring group as the acceptor, have been successfully designed, synthesized, and characterized both experimentally and computationally by Capodilupo et al [32]. The dye containing the octyloxy chains on the donor group and two thiophene ring as an extension of π-bridge showed the best photovoltaic performance with a maximum of solar energy-to-electricity conversion yield of 7.8% under AM 1.5 irradiation (100 mW/cm^2).

Zhou et al [10] synthesized Metal-Free Tetrathienoacene Sensitizers for High-Performance Dye-Sensitized Solar Cells [10]. In which they used a thiophene-based π bridge TPA-TTAR-T-A and have achieved an efficiency of 10.1%.

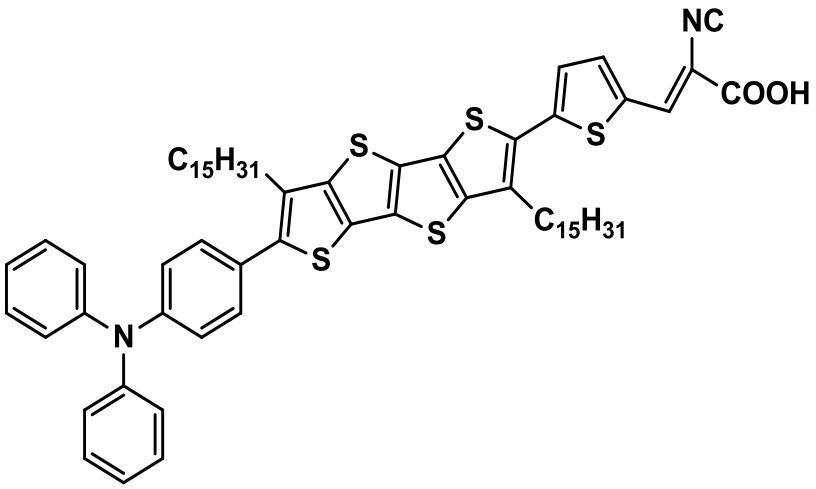

Figure 7. The structure of TPA-TTAR-T-A [10].

Mehmood et al [9] the effect of temperature on the photovoltaic performances and stability of solid-state dye-sensitized solar cells. Because the temperature is one of the most important outdoor variables that could affect the performance of the DSSCs [9].

Cui et al [51] reported the new donor-π-acceptor organic sensitizers with pyridine ring as anchoring group are designed and synthesized for p-DSSCs, their detailed investigation demonstrates that carboxylic acid groups may have an effect on the negative shift of the valence band edge of NiO induced by surface protonation, which lowers the hole-injection process and the device photovoltage, while the pyridine ring works effectively without this problem [51].

Yu et al [34] investigated the effect of anchoring groups on N-annulated perylene-based sensitizers for dye-sensitized solar cells and photocatalytic H_2 evolution [34]. In which they found that the results showed that the sensitizer with cyanoacrylic acid based DSCs showed a higher conversion efficiency of 7.58% under AM1.5 solar conditions. However, it was noteworthy to observe that the sensitizer with the rhodamine as the electron acceptor or anchoring group sensitized Pt/TiO_2 photocatalysts displayed a higher rate of H_2 evolution under visible-light irradiation with a wide absorption wavelength between 420 nm and 780 nm. The sensitizer with cyanoacrylic acid uses the COOH to attach itself to the TiO_2, while the rhodamine sensitizer binds to the TiO_2 using the NH and C=O groups [34].

Moreover in this current study the sensitizers or the synthesized dyes in like the above-mentioned rhodamine sensitizer are expected to bind to the TiO_2 semiconductor using the NH and C=O groups in their respective structures.

It has been discovered that the UV/Vis/near-IR absorption spectra of chemical compounds are likely to be influenced by the surrounding medium and that the solvents bring about a change in the position, intensity, and shape of absorption bands [35, 36]. The term solvatochromism was primarily used to describe changes in UV visible absorption band following a change in the polarity of the medium [36]. When absorption spectra are measured in solvents of different polarity it is found that not only the position but also the intensity and shape of the absorption band can vary, depending on the nature of the solvent [37, 36]. The influence of solvents on the course of chemical reactions has been studied for a long time, and efforts have been made to correlate equilibrium constants, reaction rate constants, or positions of ultraviolet absorption bands with ‘‘polarity’’ of the solvent.

Solvent polarity is very important considering the coulombic and dispersive interactions between the charge distribution in the solubility and the polarizability of the solvent. Furthermore, the electronic character of the substituent, as well as the chemistry of the solvent, are the major factors for the solvatochromic behaviour [38].

Supramolecular chemistry was first termed “the chemistry of non-covalent bonds”, these distinctive non-covalent bonding or more ion-dipole interactions, π-π^* interactions are considered as the factors that are controlling the supramolecular chemistry that deals specifically with interaction of ions with various synthetic and natural organic compounds [39]. However, these interactions have led to the development of the guest-host chemistry that further employs selective receptors (hosts) for recognition of various analyte (guest-cations, anions or biomolecules) [39, 40].

Electron transfer mechanisms such as intramolecular charge transfer (ICT) [41,42] can be employed for designing chemosensors as well as organic dyes for DSSCs. Chemosensors and organic dyes are related by the internal charge transfer mechanisms which are involved, which is the same phenomenon used in both applications. The same system of D-pi-A in Organic DSSCs is used in Chemosensors.

The general term for the host is termed as chemosensor, which is defined as devices that respond to a physical or chemical change upon its interaction with the analyte and thereby produces a signal that results from its sensitivity [43]. A chemosensor typically consists of two components; which are the binding component and the signalling component [39]. The binding component binds or interacts with the analyte by means of non-covalent interactions like van der Waals forces, hydrogen bonding etc. and this leads to chemical changes or physical changes observable like colour. Changes in the chemosensor properties can be measured using different instruments namely UV-Vis spectrophotometer and or fluorescence spectrophotometer [22].

A chemosensor should be designed in such a way that it's highly selective towards the analyte under detection even in the presence of other interfering or competing for analyte [40]. The selectivity of such chemosensor is commonly influenced by the surrounding solvent molecules, size and structural complementarity and binding strength [40].

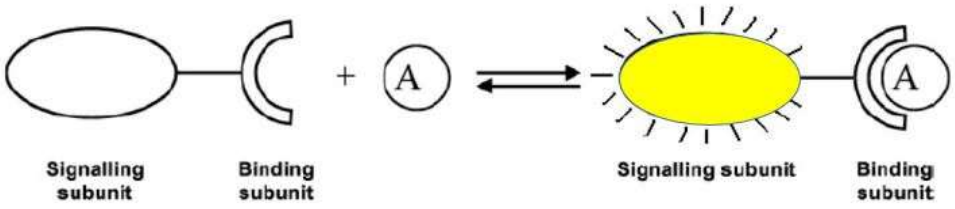

Figure 8. Schematic diagram showing binding of an analyte (guest) by a chemosensor (host), producing a complex with altered optical properties [14].

The chemosensor usually contains a chromogenic fragment and a neutral receptor with selective interactions to the visualised ion [43]. Biologically and environmentally important ions play an important role in a wide variety of organic systems, and their use in sensing and ion transport has received considerable interest in the research world [44]. Furthermore, anion chemosensor is designed in such a way that they involve three main types of interactions, which include electrostatic interactions, reaction based sensors, hydrogen bonding and metal-ligand interactions. However in recent years research has been more focused on using hydrogen bonding due to their relatively high energy, the significant availability of H-bonds donors and their strong and selective binding with anions. The commonly used anion sensors that use hydrogen bond donors with both high affinity and selectivity are amides, hydrazides, pyroles, urea and thiourea [44].

There are four essential requirements for the selection of chemo-responsive dyes, the dye should have an interaction centre that can interact strongly with the analyte, there should be a colour change after the reaction, and the interaction centre of dye must be strongly coupled to an intense chromophore, there are always a group of varied chemo-responsive dyes that are cross-responsive in a sensor array [21], and the detection results of the sensor group should be reproducible and dependable [45].

Signalling methods such as UV-visible spectroscopy, and fluorescent spectroscopy are preferred owing to their high sensitivity, this also allows low concentrations of the analyte to produce large changes in output [46]. Selectivity is considered the most

important property of a sensor, therefore it is required that the chemosensor is designed in such a way that it binds only with the desired analyte and no other competitors.

In literature, much has been done on cation and anion sensing. Cyanide [43, 33], fluoride [47], mercury [48, 50] have already been reported in literature. Subsequently, more research has been focused on urea and thiourea based anion receptors due to their ability to form strong hydrogen bonds (H-bonds) with the highly electronegative anions like fluoride [40, 32].

Zhang et.al, [33] designed a highly selective and sensitive chemosensor for instant detection cyanide via different channels in aqueous solution. This sensor probe displayed rapid response and high selectivity for cyanide over other common ions in aqueous solution [33]. Cyanide (CN^-) being one of the most toxic anions, which is also deadly to human beings as it affect many functions in the human body, which includes the visual, central nervous, vascular, cardiac, endocrine and metabolism systems. Therefore sensitive, simple and affordable sensors for cyanide are necessary and are in demand. However up to date a large number of chemosensors for CN^- have been developed [51].

Lee et al [48] reported the chemosensing properties and characteristics of squarylium-based chemosensors for Hg^{2+}. This dye was found to be only selective to the sensing of mercury (Hg^{2+}). However, earlier Lee et. al, [48] reported the synthesis and binding properties of this dye chemosensor which exhibited high selectivity for cyanide anion (CN^-) among other anions. This clearly indicates the dual sensitivity of this particular sensor.

Thiophene-based metal free dye sensitizers have already been reported in the literature and they show promising efficiencies of about 10.5% [18]. However, sensing

properties on this metal-free dyes for DSSCs have not yet been investigated. Even though sensors containing thiophene has been previously reported [49]. So far these sensors were also not tested for their DSSCs properties. However little or nothing has been done regarding the chemosensing properties of the organic based DSSCs. Hence in this area research is to be done. Therefore studies that are focused on investigating both DSSC properties and chemosensing properties are vital and will be done in this particular research.

CHAPTER 3: RESEARCH METHODS

3.1 Research design

Two facile metal free dyes sensitizers were designed and synthesized. These dyes were then characterised using UV spectroscopy, FT IR, ^{1}H-NMR and fluorescence, and their optical, electronic and chemosensing properties were also studied.

3.2 Procedures

3.2.1 Materials

All starting materials and solvents used in this research were of analytical grade.

3.2.2 Organic dye I1

The organic dye I1 was synthesized by a simple Schiff base reaction. To a solution of 2-aminothiazole (2.0020g, 0.02 mol) in ethanol 60ml, a solution of Isatin (2.9425g, 0.02 mol) in ethanol 20ml was added dropwise while magnetically stirring under reflux for 5 hours. Mass of the product 5.2321g. Yield 73 %, IR **(**cm $^{-1}$): 1300- 1550 , 1720-1726, 3201.1, and ^{1}H NMR(400 MHz, $CDCl_3$), δ: 7.67 ppm (s, NH), 6.97 ppm (d, 1H, 2-thiophene), 7.45 ppm (d, 1H, 3-thiophene), 7.57 ppm (m, 1H, ArH), 6.84 ppm (m, 1H, ArH), 7.06 ppm (m,1H, Ar-H), 7.50 ppm (m, 1H, ArH).

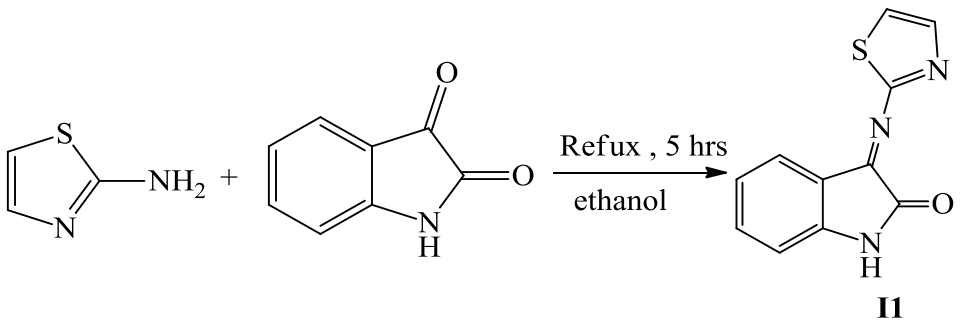

I1

Scheme 1. The synthetic route of Dye **I1**

3.2.3 Organic dye I2

Organic dye I2 was synthesized in two steps

Isatin (2.0023g, 0.014 mol) hydrazine monohydrate (2.0048g, 0.014 mol) and a catalytic amount of acetic acid (five drops of AcOH) were combined in 60 ml of absolute ethanol. The solution was stirred under reflux for 4 hours. After cooling at room temperature, a yellow precipitate was filtered, washed three times with hot absolute ethanol. Mass of product 1.4536g.

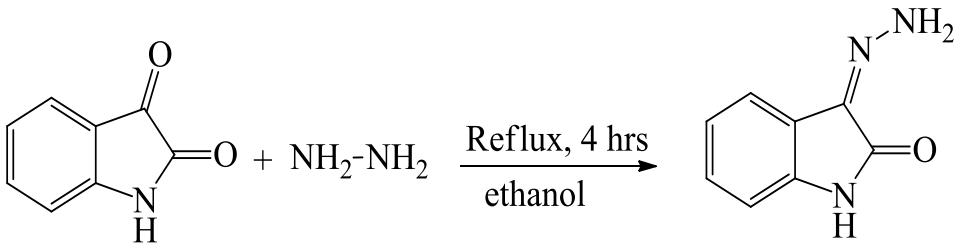

Scheme 2. The synthetic route of dye I2 the intermediate step

Synthesis of dye I2

The product obtained in step 1 (1.0299g, 0.0062 mol), 2-hydroxy-1-naphthaldehyde (1.0674g, 0.0062 mol) and a catalytic amount of H_3PO_4 (3 drops) were combined in absolute ethanol 60 ml. The solution was stirred under reflux for 5 hours. It was then cooled at room temperature, and an orange precipitate was filtered off, washed three times with hot absolute ethanol. The mass of the product 1.5130g. Chemical shifts are reported in ppm relative to tetramethylsilane δ units as the internal standard. Yield 77%, IR (cm^{-1}): 3169-3800, 1290- 1524, 1720-1722.2, 3676.9

, and ^1H NMR (400 MHz, $CDCl_3$), δ: 14.35 ppm (s, H), 7.02 ppm (s, OH), 7.55 ppm (s, NH), 9.7 ppm (dd, 1H, naphthalene-H), 8.2 ppm (dd, 1H, naphthalene-H), 7.9 ppm

(m, 1H, naphthalene-H), 7.0 ppm (m, 1H, Ar-H), 6.9 ppm (m, 1H, Ar-H), 7.5 ppm (m, 1H,ArH), 7.15 ppm (m, 1H, ArH), 7.8 ppm (m, naphthalene-H), 7.6 ppm (m, 1H,naphthalene-H), 7.25 ppm (m, 1H, naphthalene-H).

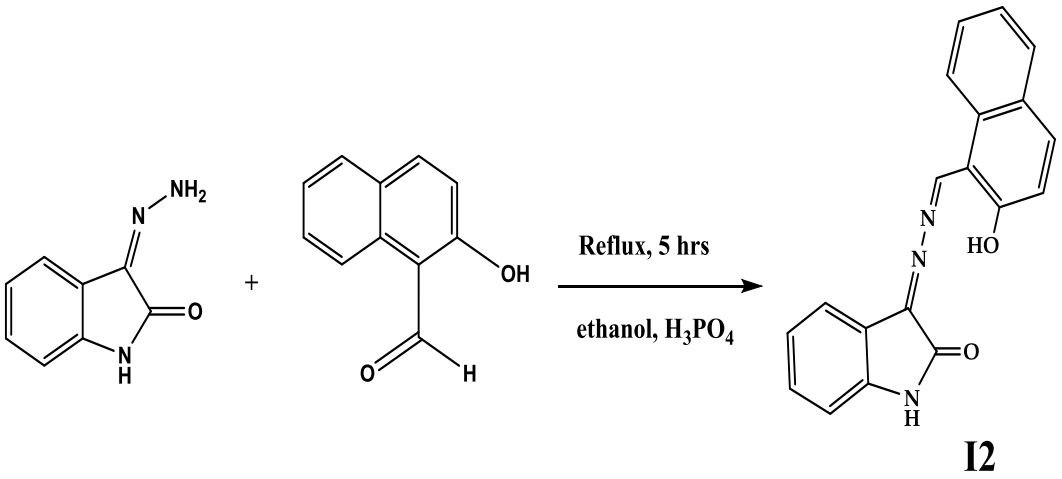

I2

Scheme 3. The synthetic route of dye I2 step 2

3.2.5 General procedures for the UV-vis titration experiments

All the UV-vis experiments were carried out in DMSO solution on a UV-vis spectrophotometer. The changes in the UV-vis spectra of the synthesized dye were recorded upon addition of tetrabutylammonium (TBA) salts of anions as well as the cation salts of chlorides and nitrates. While keeping the concentration of the dyes constant (1×10^{-5} M). In all experiments TBA salts of anions (F^-, Cl^-, AcO^-, CN^-, Br^-, N_3^-, SO_4^{2-}, NO_3^-) as well as the chloride and nitrate salts of cations (Mn^{2+} , Ba^{2+} , Co^{2+}, Fe^{2+}, Ag^+, Fe^{3+}, Zn^{2+}, Al^{3+}, Pb^{2+}, Cu^{2+}, Hg^{2+}, Cr^{3+}, Na^+) were used.

3.2.6 General procedures for fluorescence spectra experiments

All fluorescence spectroscopy was carried out in DMSO solution on the fluorescence spectrometer. Any change in the fluorescence spectra of the synthesized dye were recorded on the addition of the TBA salts and as well as the salts of chloride and nitrate,

while keeping the concentration of the dyes constant at ($1*10^{-5}$ M). In all experiments TBA salts of anions (F^-, Cl^-, AcO^-, CN^-, Br^-, N_3^-, SO_4^{2-}, NO_3^-) as well as the chloride and nitrate salts of cations (Mn^{2+} , Ba^{2+} , Co^{2+}, Fe^{2+}, Ag^+, Fe^{3+}, Zn^{2+}, Al^{3+}, Pb^{2+}, Cu^{2+}, Hg^{2+}, Cr^{3+}, Na^+) were used in a constant concentration of 0.3 M.

3.2.7 General preparation of the solvatochromism dyes

The dyes for solvatochromism were prepared in different solvents (methanol, chloroform, tetrahydrofuran, acetone, dichloromethane, toluene, ethyl acetate, ethanol, n-hexane and DMSO) while keeping the concentrations constant in both solvents ($1*10^{-5}$ M).

CHAPTER 4: RESULTS AND DISCUSSION

4.1 The photophysical properties of the dyes

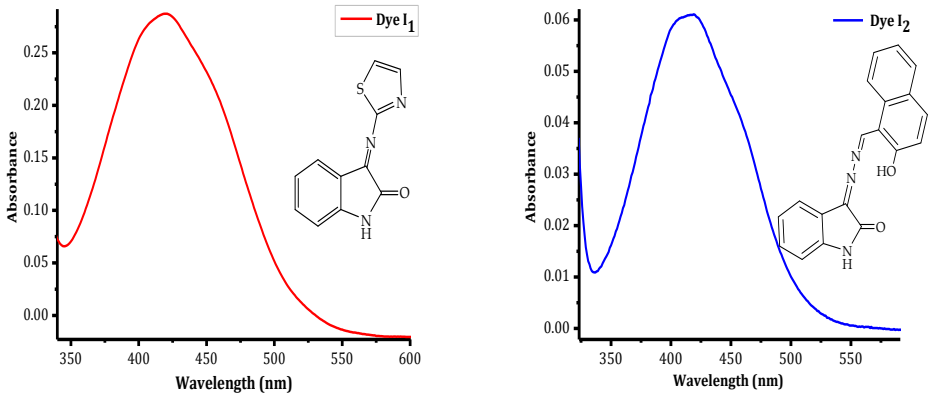

(a) (b)

Figure 9. UV-Vis spectra of (a) Dye I1 (b) Dye I2 at a concentration of ($1*10^{-5}$ M) in DMSO

The absorption wavelength of Dye I1 is 340-550nm, Dye I2 is 350-550nm. Which is recognized to be caused by the intramolecular charge transfer (ICT) of the dye. The results of the absorption wavelength showed that the dyes solution in Figure 9 can be used as photosensitizer for DSSC because they both have absorption bands that appeared in the visible region of the absorption spectrum.

4.1.2 HOMO-LUMO energy gap studies

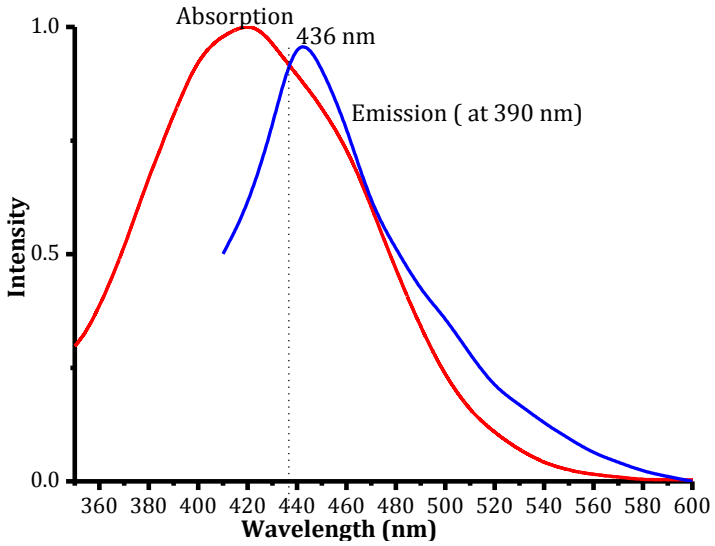

Figure 10. The normalized absorption and emission spectra of dye I1

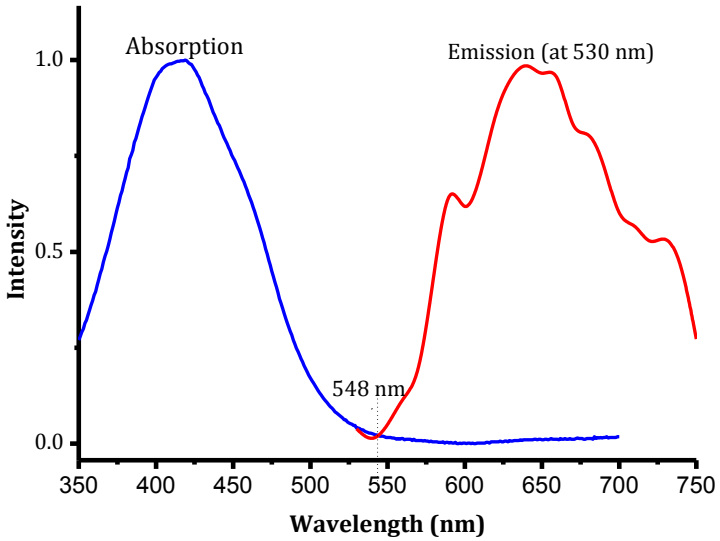

Figure 11. The normalized absorption and emission spectra of dye I2

The HOMO-LUMO energy gap E_{H-L} of dye I1 and dye I2 were estimated by the intersection point between their normalized absorption and emission spectra of the dyes **I1** and **I2** as shown in figure 11 and 12 respectively, and it was calculated from the following equation:

$$E_{H-L}/\ eV = 1240/\ (\lambda/nm)$$

In dye **I1** the intersection wavelength is 438 nm, while for dye **I2** the intersection wavelength is 548 nm, therefore the HOMO-LUMO gaps for dye **I1** and dye **I2** were calculated using the above equation and determined to be 2.84 eV and 2.26 eV respectively. These dyes all have narrow HOMO-LUMO gaps which is less than 3 eV, this means that these dyes are expected to capture more light in the visible region. Since their band gap is narrow, thus lowest band gap of dye helps the electron move fast from the valence band to the conduction band they are suitable for use in solar cells.

4.1.3 Structure elucidation

4.1.3.1 The FTIR studies

I1- The remarkable peaks in the FTIR spectra of **I1** also occur at a wavenumber of 1300- 1550 cm^{-1}, 1720- 1726 cm^{-1} and 3201.1 cm^{-1} which correspond to C=C aromatic, and C=O stretch vibration and N-H , respectively.

I2- The wide vibrational range at a wavenumber of 3169-3800 cm^{-1} corresponds to the O-H stretching vibration. The remarkable peaks in the FTIR spectra of dye **I2** also occur at a wavenumber of 1290- 1524 cm^{-1}, 1720-1722.2 cm^{-1} and at 3676.9 cm^{-1} which correspond to, C=C aromatic, and C=O stretch vibration, and N-H stretch respectively.

4.1.3.2 Interpretation of the ^{1}H NMR results

Table 1. The ^{1}H-NMR results of dye I1

Chemical shifts (ppm)	Multiplicity	Integration
6.84	m	1H
6.97	d	1H
7.06	m	1H
7.45	d	1H
7.50	m	1H
7.57	m	1H
7.67	s	NH

Table 2. The ^{1} H-NMR for dye I2

Chemical shifts (ppm)	Multiplicity	Integration
6.9	m	1H
7.0	m	1H
7.02	s	OH
7.15	m	1H
7.25	m	1H
7.5	m	1H
7.55	s	NH
7.6	m	1H
7.8	m	1H
7.9	m	1H
8.2	m	1H

9.7	m	2
14.35	s	H

4.2 Solvatochromism

The solvatochromic effects of dye I1 were investigated in different solvents of different polarity. The absorption spectra were recorded in nine different solvents of varying polarities at room temperature. The solvatochromic effects on absorption spectra have shown a hypochromic effect in DMSO solution as well as a bathochromic (red shifted). Clearly, the absorption spectra of the dyes I1 in DMSO solution are red-shifted as compared to the dye spectra in other solutions, indicating relatively strong guest-host interaction between the dye molecules and the DMSO environment, while some solvents such as acetone, chloroform, ethyl acetate, EtOH, MeOH, and THF showed a hypochromic effect as well as a bathochromic shifts. However, this particular dye was extremely hypochromic shifted in low polarity solvents like n-hexane, toluene and DCM.

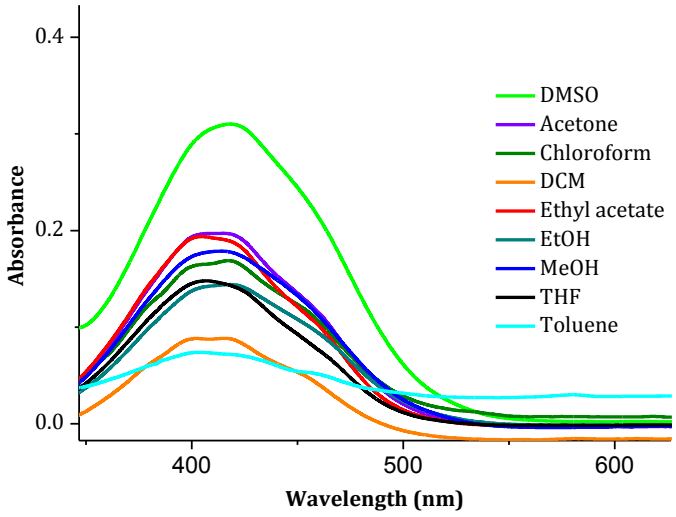

Figure 12. Shows the solvatochromism effects of the solvents on dye I1.

The solvatochromic effects of dye I2 were investigated in different solvents of different polarity. The absorption spectra were recorded in these nine different solvents with increasing polarities at room temperature. The solvatochromic effects on

absorption spectra have shown a hypochromic effect in toluene solution, while some solvents showed such as EtOH, MeOH it shows a bathochromic (redshifted) shift, while chloroform and DCM show hypochromic as well as bathochromic shifts. Effect as well as a bathochromic shift. Moreover, ethyl acetate, DMSO, DCM, and acetone only showed hypochromic shifts.

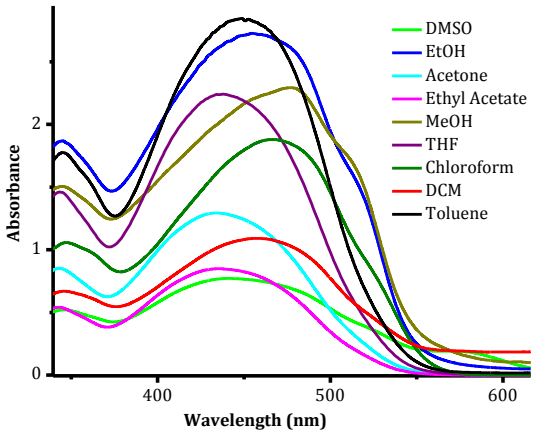

Figure 13. Shows the solvatochromism effects of the solvents on dye I2.

4.3 Interaction studies of the sensors with analytes

The binding properties of the two dyes have been investigated by UV/Vis absorption and fluorescence spectroscopy. The titration experiments have been carried out in DMSO system at room temperature with 0.03 M to keep a constant ionic strength. The chloride, fluoride and nitrate salts of Mn^{2+} , Ba^{2+} , Co^{2+}, Fe^{2+}, Ag^{+}, Fe^{3+}, Zn^{2+}, Al^{3+}, Pb^{2+}, Cu^{2+}, Hg^{2+}, Cr^{3+}, Na^{+} as well as the TBA salts of the anions (F^{-}, Cl^{-}, AcO^{-}, CN^{-} , Br^{-}, N_3^{-}, SO_4^{2-}, NO_3^{-}) were used.

4.3.1 Interaction of Sensor A with anions and cations

The ability of **sensor A** to complex with various anions was studied by UV-vis absorption. Upon addition of Hg^{2+} into a DMSO solution of **sensor A**, is characterized by two absorption band in the visible region, the weak and intense bands at 400 nm and 496 nm, respectively. In contrast, other competing cations and anions such as Mn^{2+} , Ba^{2+} , Co^{2+}, Fe^{2+}, Ag^{+}, Fe^{3+}, Zn^{2+}, Al^{3+}, Pb^{2+}, Cu^{2+}, Cr^{3+}, Na^{+} and F^{-}, Cl^{-}, AcO^{-}, CN^{-}, Br^{-}, N_3^{-}, SO_4^{2-}, NO_3^{-} respectively are completely unresponsive. These results indicated implied the selectivity and sensitivity of **sensor A** towards Hg^{2+}. Corresponding colour response of **sensor A** with different cations was observed. In addition to spectral changes when Hg^{2+} was added to the solution of **sensor A,** it led to a colour change from pale yellow to colourless which could be detected with the naked eye. The interaction is suspected to be of the coordination nature involving cationphilic neighbouring atoms (Sulphur and Nitrogen) and the Mercury ion (Hg^{2+}). The UV-vis response of **sensor A** towards Hg^{2+} was investigated in DMSO as shown in figure 14.

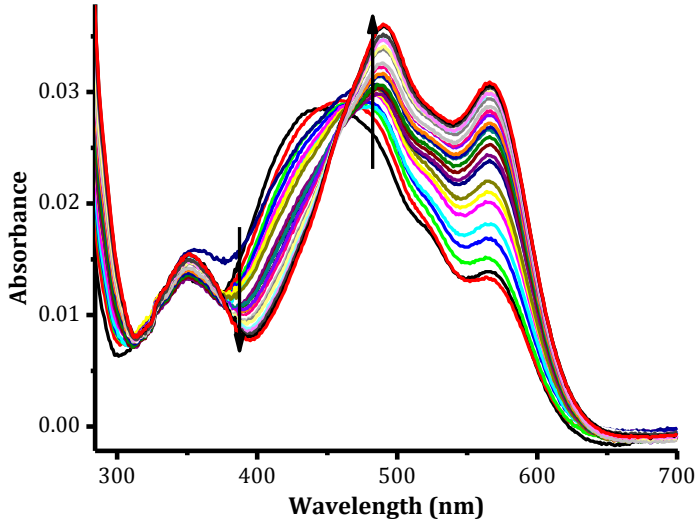

Figure 14. The titration of **sensor A** ($1x10^{-5}$ M) in the presence of Hg^{2+} cation (0. to 5.0 equiv.) in DMSO solution.

4.3.2 Interaction of Sensor B with anions and cations

As the CN^- concentration increases, the absorbance of **sensor B** at 450 nm decreased significantly and a new absorption peak appeared at 560 nm with a sharp isosbestic point formation at 500 nm, which indicates that only two species are present at the equilibrium throughout the titration process. In contrast, upon addition of other competing anions such as Cl^-, AcO^-, Br^-, N_3^-, SO_4^{2-}, NO_3^- and cations such as Mn^{2+}, Ba^{2+}, Co^{2+}, Fe^{2+}, Ag^+, Fe^{3+}, Zn^{2+}, Al^{3+}, Pb^{2+}, Cu^{2+}, Cr^{3+}, Na^+ no detectable changes were observed. The corresponding colour response of **sensor B** with different cations was also tested. When CN^- was added to the solution of **sensor B**, it resulted in a colour change from pale yellow to colourless which could be detected with the naked eye. It is well known that the interaction of anions is with hydrazone moiety is through hydrogen bonding with the NH proton, as well as the OH proton in the **sensor B.** The UV-vis response of **sensor B** towards CN^- was investigated in DMSO as shown in figure 15.

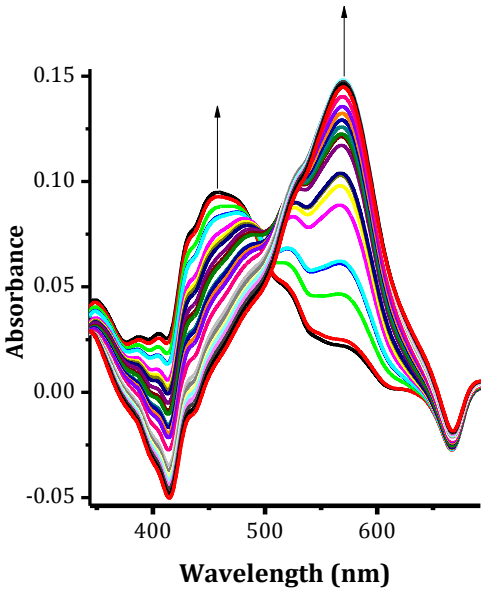

Figure 15. The titration of **sensor B** (1 x 10^{-5} M) in the presence of CN^- anion (0-5.0 equiv.) in DMSO solution.

To investigate the binding mode of **sensor B** with F^-, titrations were performed, upon the addition of 0-0.5 equivalent. F^-, the absorbance of **sensor B** at 460 nm gradually decreased, meanwhile, the absorbance of **sensor B** at 590 nm gradually increased. The well-defined isosbestic points at 480 nm and at 670 nm clearly indicate the existence of two distinct species at equilibrium during the titration process. In contrast, other competing anions such as Cl^-, AcO^-, Br^-, N_3^-, SO_4^{2-}, NO_3^- and cations such as Mn^{2+}, Ba^{2+}, Co^{2+}, Fe^{2+}, Ag^+, Fe^{3+}, Zn^{2+}, Al^{3+}, Pb^{2+}, Cu^{2+}, Cr^{3+}, Na^+ were completely non-responsive and did not induce any significant or noticeable changes. When F^- was added to the solution of **sensor B** it led to a colour change from pale orange to purple which could be detected with the naked eye. The UV-vis response of **sensor B** towards F^- was investigated in DMSO as shown in figure 16.

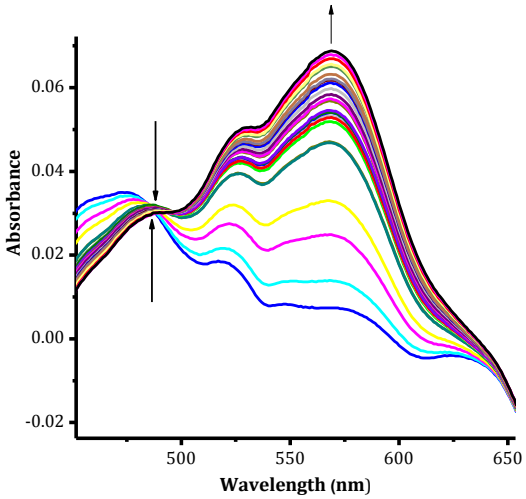

Figure 16. The titration of **sensor B** (1 x 10^{-5} M) in the presence of F^- anion (0-5.0 equiv.) in DMSO solution.

4.4 The Fluorescence studies

4.4.1 Interaction of Sensor A with anions and cations

Fluorescence emission spectra were recorded upon excitation at 430 nm, the fluorescence intensity steadily increased at 440 nm. The fluorescence of the **sensor A** was enhanced by the introduction of Hg^{2+}, hinting that the sensor could be applied for sensing Hg^{2+}. Further, the selectivity of the sensor for sensing mercury ions was investigated, the addition of various anions such as CN^-, Cl^-, AcO^-, Br^-, N_3^-, SO_4^{2-}, NO_3^-, F^- and cations such as Mn^{2+}, Ba^{2+}, Co^{2+}, Fe^{2+}, Ag^+, Fe^{3+}, Zn^{2+}, Al^{3+}, Pb^{2+}, Cu^{2+}, Cr^{3+}, Na^+ exhibited no all small significant increase of the fluorescence. This results indicated that the fluorescent probe had favourable sensitivity and selectivity for the detection of Hg^{2+}.

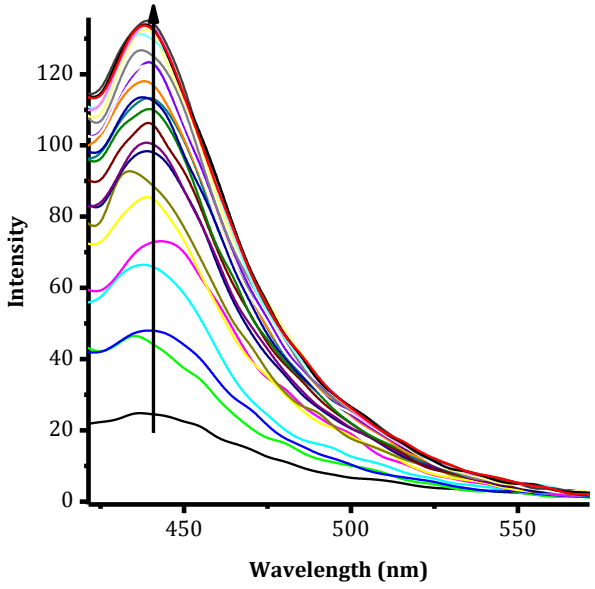

Figure 17. Fluorescence spectra of **Sensor A** on the molar addition of a different amount of Hg^{2+} in DMSO (from 0-5 equiv.).

4.4.2 Interaction of Sensor B with anions and cations

Fluorescence emission spectra were recorded upon excitation at 430 nm, the fluorescence intensity steadily increased at 460 nm. The fluorescence of the **sensor B** was enhanced by the introduction of CN^-, suggesting that the sensor could be applied for sensing CN^-. Further, the selectivity of the **sensor B** for sensing CN^- was investigated, the addition of various anions such as Cl^-, AcO^-, Br^-, N_3^-, SO_4^{2-}, NO_3^-, F^- and cations such as Mn^{2+}, Ba^{2+}, Co^{2+}, Fe^{2+}, Ag^+, Fe^{3+}, Zn^{2+}, Al^{3+}, Pb^{2+}, Cu^{2+}, Cr^{3+}, Na^+ exhibited no significant increase of the fluorescence while F^- showed a significant change on the fluorescence spectra. These results indicated that the fluorescent probe had favourable sensitivity and selectivity for the detection of CN^- and F^-.

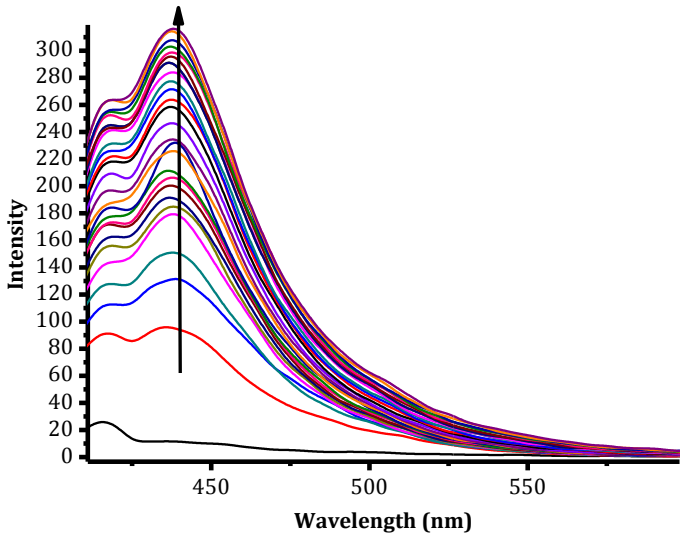

Figure 18. Fluorescence spectra of **Sensor B** on the addition of a different amount of CN^- in DMSO (from 0-5 equiv.).

Fluorescence emission spectra were recorded upon excitation at 425 nm, the fluorescence intensity steadily decreased at 450 nm. The fluorescence of the **sensor B** was quenched by the introduction of F^-, suggesting that the sensor can also be applied for sensing F^-.

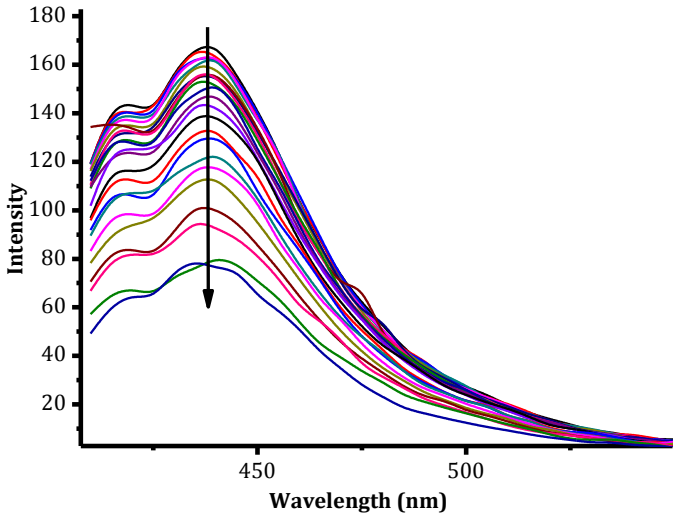

Figure 19. Fluorescence spectra of **sensor B** on the addition of a different amount of F^- in DMSO (from 0-5 equiv.).

4.5 The proposed binding mechanism of the sensors and the ions

4.5.1 Binding mechanism for sensing of Hg^{2+} with sensor A

It is proposed that **sensor A** binds with Hg^{2+} through the nitrogen and sulphur atom, the interaction is suspected to be of coordination nature involving two intermediate cationphilic neighbouring atoms (sulphur and nitrogen) and the Hg^{2+} [52] forming a 1:1 reaction as shown in scheme 4. When Hg^{2+} ions were added to **sensor A**, the sensor changed colour from yellow to pale yellow.

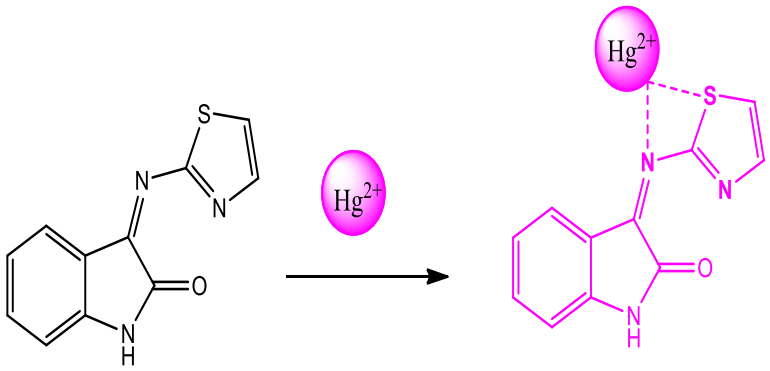

Scheme 4. Proposed binding Mode of **sensor A** with Hg^{2+}.

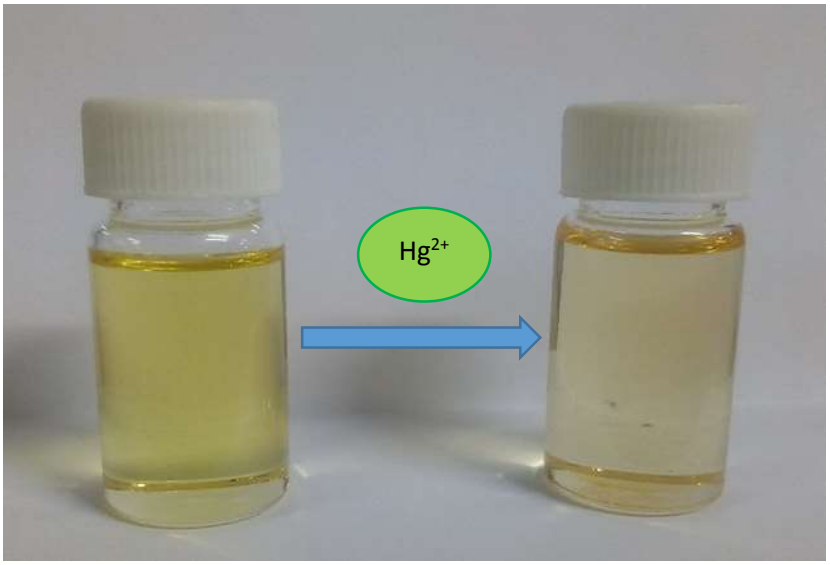

Scheme 5. The naked eye detectable change of **sensor A** with Hg^{2+}.

4.5.2 Binding mechanism for sensing of CN^- with sensor B

It is proposed that **sensor B** binds with CN^- through the amine and hydroxide protons, forming a 1:2 reaction as shown in scheme 8. Detectable colorimetric change were observed with naked eye when CN^- ions were added to **sensor B**, the sensor changed colour from pink to purple as shown in scheme 8.

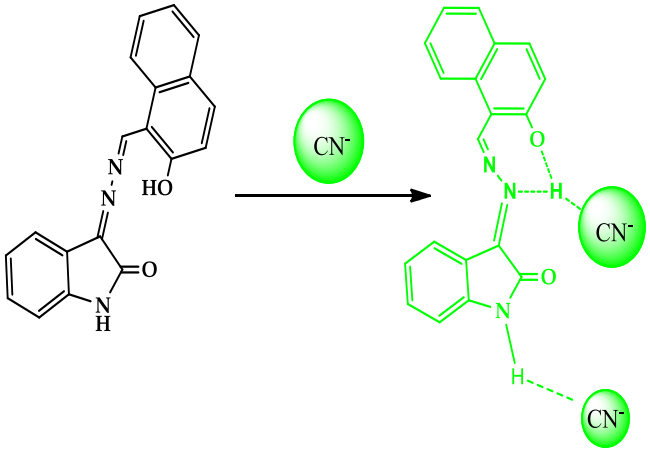

Scheme 6. The proposed binding mode of **sensor B** with CN^-.

It is proposed that **sensor B** binds with F^- through hydroxide protons, forming a 1:1 reaction as shown in scheme 8. The sensing of the CN^- anion was probably formed via the H-bonding of the CN^- anion to the OH of the **sensor B** [33], which could as well be via the H-bonding of the CN^- anion to the NH of the **sensor B** [49]. Detectable colorimetric change was observed with naked eye when F^- ions were added to **sensor B**, the sensor changed colour from pink to purple as shown in scheme 8.

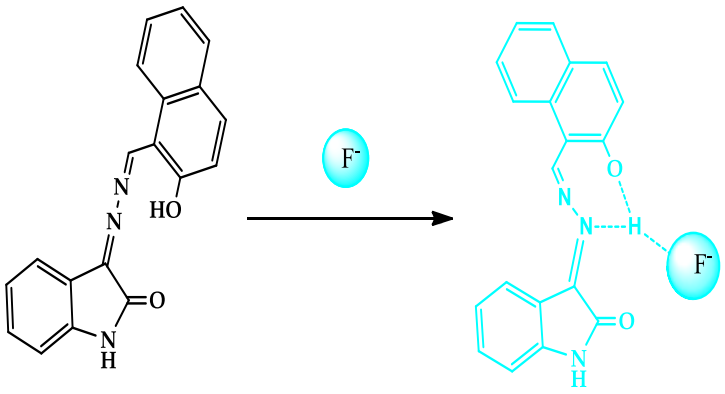

Scheme 7. The proposed binding mode of **sensor B** with F^-.

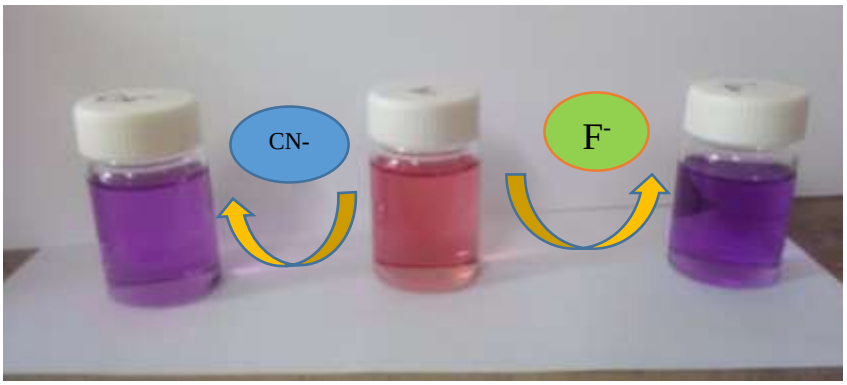

Scheme 8. The naked eye detectable change of **sensor B** with CN^- and F^-.

4.6 The Job plot studies

4.6.1 The interaction ratio of Hg^{2+} with sensor A

To understand the binding stoichiometry between **sensor A** and Hg^{2+} Job's plot experiment was carried out. As shown in figure 20, the profile indicates a 1:1 stoichiometry for the process, these results are in agreement with the proposed binding mode of **sensor A** with Hg^{2+}.

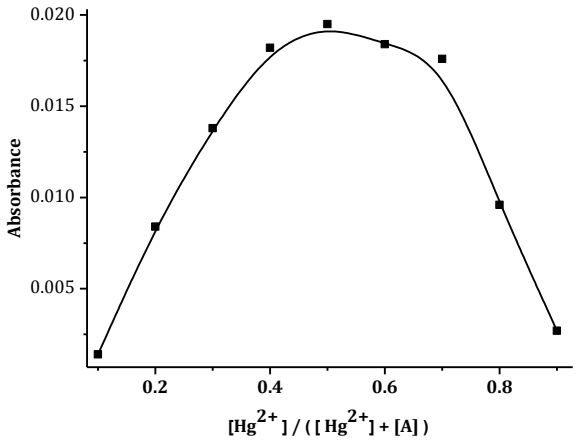

Figure 20. The Job's plot examined between Hg^{2+} and **sensor A** indicating a 1:1 stoichiometry.

4.6.2 The interaction ratio of CN^- with sensor B

As the expected nucleophilic attack on unsaturated bond groups of **sensor B** should satisfy 1:2 probe and cyanide stoichiometry. The results obtained from the job's plot supports the formation of a 1:2 **sensor B**/ CN^- adduct as shown in figure 21.

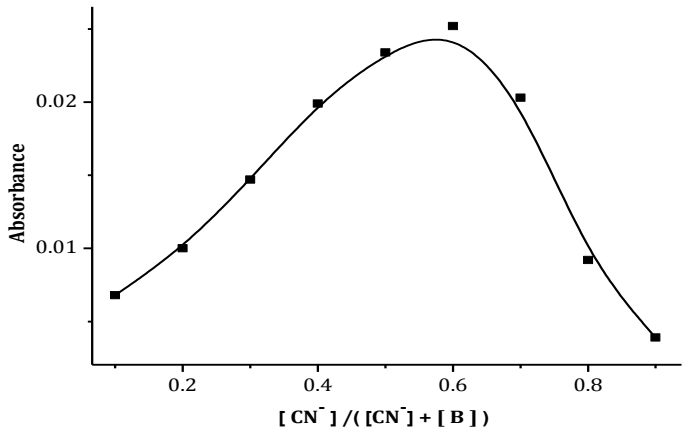

Figure 21. The Job's plot examined between CN^- and **sensor B** indicating a 1:2 stoichiometry.

4.6.3 The interaction ratio of F^- with sensor B

The reaction between **sensor B** and F^- gave a 1:1 stoichiometric ratio, however it was this reaction could also have resulted into a 1:2 stoichiometric ratio, because F^- can either deprotonate the N-H and O-H fragments in which the anion takes a proton from the receptor. So in this case, this 1:1 stoichiometric ratio could be due to the deprotonation of one of the above-mentioned fragments. It is suggested that the high selectivity might be attributed to the strong intramolecular N-H···O hydrogen bonding of **sensor B** from which the hydrogen atom was fastened, and only the anion showing the most electronegative property had the potential to form additional hydrogen bonding [47].

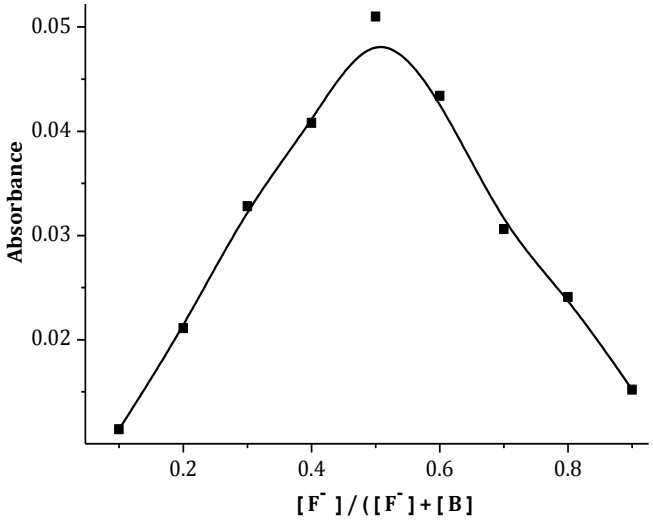

Figure 22. The Job's plot examined between F^- and **sensor B** indicating a 1:1 stoichiometry

CHAPTER 5: CONCLUSION AND RECOMMENDATIONS

5.1 Conclusions

In summary, two facile, low cost, and efficient Schiff base dyes are reported. Dye I1 being a thiophene-based metal-free organic dye for DSSCs as well as dye I2 that was used for comparison, which were synthesized through facile Schiff-base condensation reactions. A thiophene dye was successfully synthesized and characterized, this dye I1 had very good characteristics of light absorption in the visible region with a broad absorption band ranging from 340-550 nm. In comparison, another dye I2 was synthesized. Solvatochromic effects of the dyes were carried out to find out the best solvent to dissolve these dyes for analysis. To find this out, the absorption spectra were measured in solvents of different polarity. It is found that not only the position but also the intensity and shape of the absorption band can vary, depending on the nature of the solvent. Since all the two dyes gave very broad peaks in the visible region of the spectrum when dissolved in DMSO solvent, this solvent was used for the UV-vis and fluorescence analysis. The HOMO-LUMO gap of these two dyes I1 and I2 were determined to be 2.84, and 2.26 eV respectively. Since these calculated band gaps are narrow, these dyes are expected to capture a reasonable amount of sunlight within the visible region of the solar spectrum, and thus they are suitable for the use in DSSCs.

For structure elucidation, FT-IR was carried out to confirm the structure of the dyes, as well as the ^{1}H-NMR spectra's. The insert shows the FT-IR and the ^{1}H-NMR spectra's of both dye I1 and dye I2 respectively. The functional groups in the FT-IR spectra were identified and thus they confirm the synthesized structures of the dyes. Furthermore, their signals in the ^{1}H-NMR spectra's were also identified, and they also further confirmed the speculated structures of these dyes.

These dyes were tested for their chemosensing properties with dye I1 being **sensor A** and dye I2 being **sensor B**. The **sensor A** showed very effective detection behaviours of UV–vis absorption by the addition of Hg^{2+} cation. This **sensor A** was only responsive to Hg^{2+} cation, thus it's only specific for this particular ion which makes it a very good sensor, since its highly selective towards the analyte (Hg^{2+}) under detection even in the presence of other interfering or competing for an analyte. This chemosensors that are selective for specific targets of metal ions are continuously in demand. While **sensor B** was able to detect CN^- and F^-, thus **sensor B** is a dual-sensor that detects two anions, this **sensor B** may contribute to the efficient dual-sensing colorimetric chemosensors. Therefore these dyes can both be used as chemosensor as they show a high potential in supramolecular chemistry.

The fluorescence results are in agreement with the UV-vis results, as they showed **sensor A** showed fluorescence enhancement for Hg^{2+}, while **sensor B** showed fluorescence enhancement with cyanide (CN^-) and fluorescence quenching with fluoride (F^-) anions.

In order to understand the binding modes of the ions, the jobs plot analysis were obtained. Results indicate that for the reaction between **sensor A** and Hg^{2+} ion, the reaction ratio is 1:1 which is in agreement with literature that the interaction is suspected to be of coordination nature involving two intermediate cationphilic neighbouring atoms (sulphur and nitrogen) and the mercury ion [49]. While the reaction between **sensor B** and CN^- ion is a 1:2 which implies that the sensing of the CN^- anion was probably formed via the H-bonding of the CN^- anion to the OH of the **sensor B** [33], as well as via the H-bonding of the CN^- anion to the NH of the **sensor B** [44]. The reaction between **sensor B** and F^- gave a 1:1 stoichiometric ratio, which evidences the fact that fluorine is an electronegative atom, and rightfully establishes

the H-bond interactions, and it does so by deprotonation of the N-H and O-H fragments in which the anion takes a proton from the receptor [43]. To sum up each dye possesses a duality function, as an organic DSSC as well as a colorimetric sensors for discriminating specific ionic species in a given environment.

5.2 Recommendations

Solar cells based on the dyes in this study should be carried out to determine the efficiency of these synthesized dyes.

APPENDICES

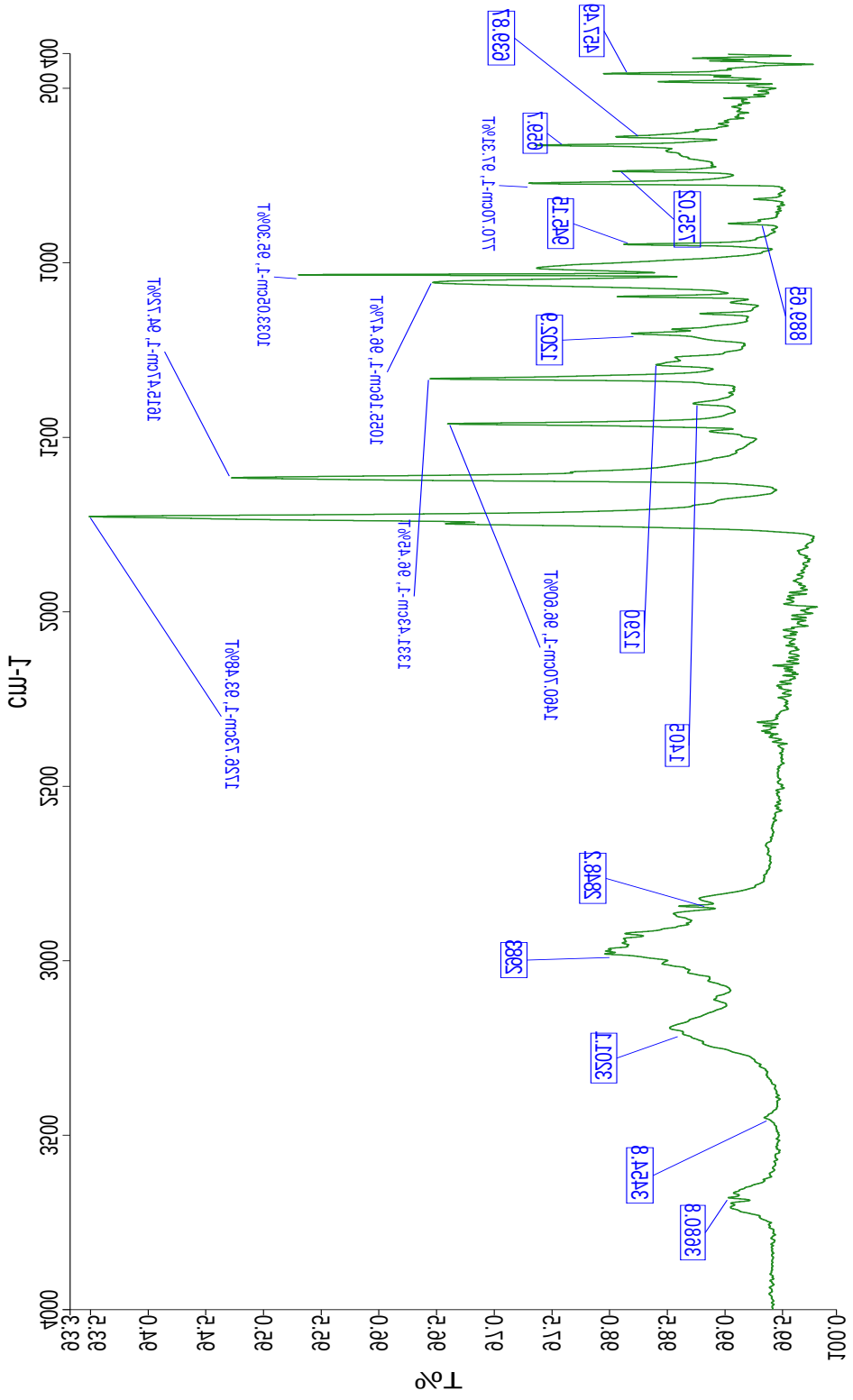

Figure 23. The FT-IR spectrum of Dye I1.

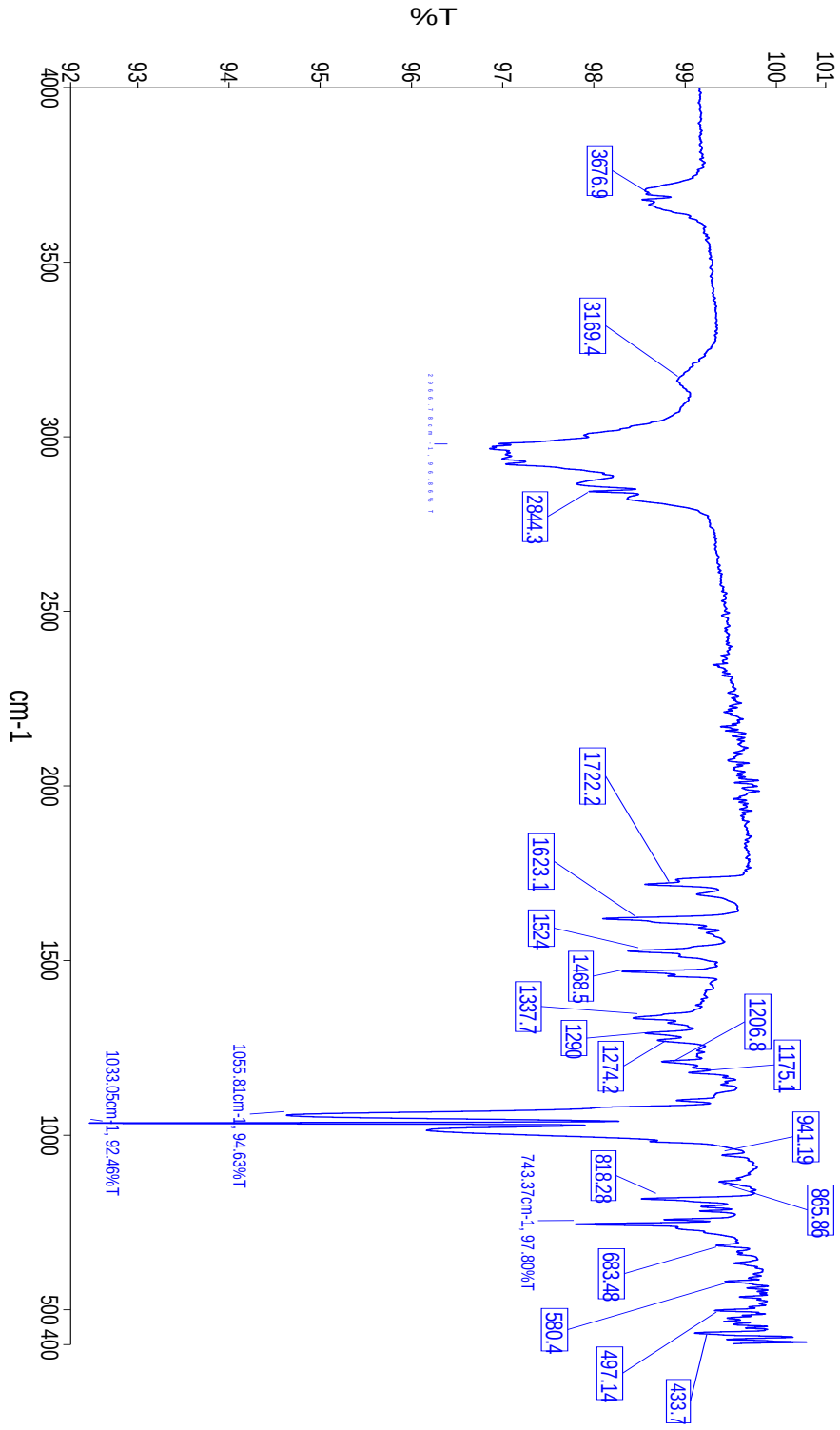

Figure 24. The FT-IR spectrum of Dye I2.

I1

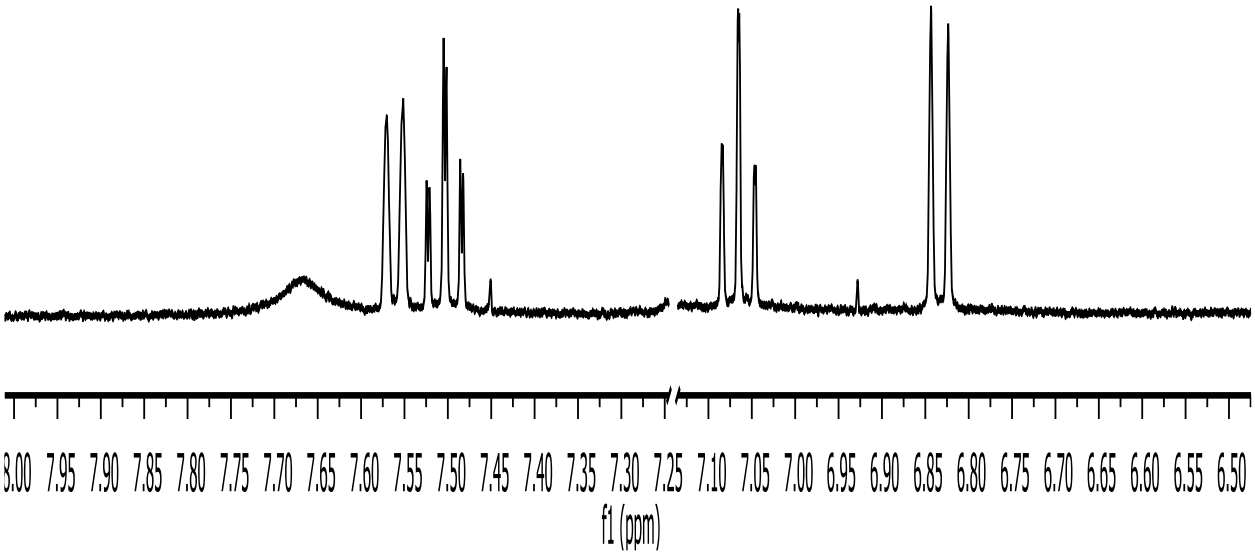

Figure 25. The ^{1}H NMR spectra of Dye I1.

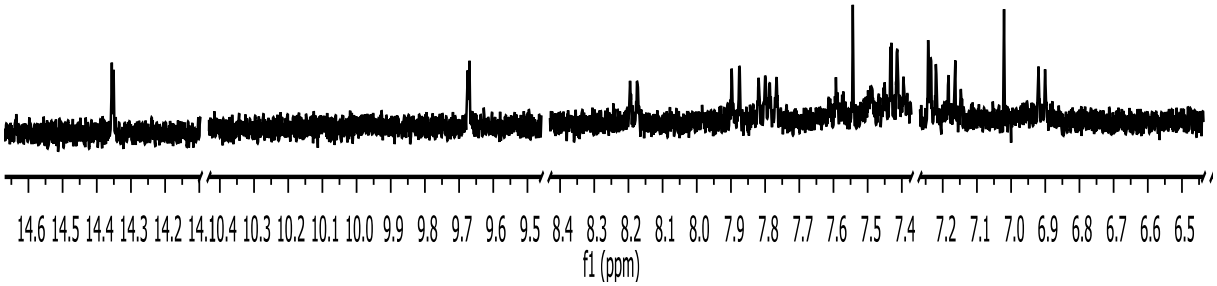

Figure 26. The ^{1}H NMR spectra of Dye I2.

CHAPTER 6: REFERENCES

[1]. Mishra A, Fischer MK, Bäuerle P. Metal-free organic dyes for dye-sensitized solar cells: From structure: Property relationships to design rules. *Angewandte Chemie International Edition*. 2009; 48(14): 2474-2499.

[2]. Fernandes SS, Castro MC, Mesquita I, Andrade L, Mendes A, Raposo MM. Synthesis and characterization of novel thieno [3, 2-b] thiophene based metal-free organic dyes with different heteroaromatic donor moieties as sensitizers for dye-sensitized solar cells. *Dyes and Pigments*. 2017; 136: 46-53.

[3]. Capuano L. International energy outlook 2018 (IEO2018). US Energy Information Administration (EIA): *Washington, DC, USA*. 2018 Jul 24; 2018:21.

[4]. Richhariya G, Kumar A, Tekasakul P, Gupta B. Natural dyes for dye-sensitized solar cell: A review. Renewable and Sustainable *Energy Reviews*. 2017; 69:705-718.

[5]. Khan HZ, Al-Mamun MR, Halder PK, Aziz MA. Performance improvement of modified dye-sensitized solar cells. *Renewable and Sustainable Energy Reviews.* 2017; 71: 602-617.

[6]. Different Types of Renewable Energy Sources And Their Benefits. Web blog. [Online]. Available from: https://thesmallbusinessblog.net/different-types-of-renewable-energy-sources-and-their-benefits/ [accessed 13th May 13, 2019].

[7]. Sugathan V, John E, Sudhakar K. Recent improvements in dye-sensitized solar cells: A review. *Renewable and Sustainable Energy Reviews*. 2015; 52:54-64.

[8]. Kibria MT, Ahammed A, Sony SM, Hossain F, Islam SU. A Review: Comparative studies on different generation solar cells technology. *In Proc. of 5th International Conference on Environmental Aspects of Bangladesh*. 2014.

[9]. Mehmood U, Al-Ahmed A, Al-Sulaiman FA, Malik MI, Shehzad F, Khan AU. Effect of temperature on the photovoltaic performance and stability of solid-state dye-sensitized solar cells: A review. *Renewable and Sustainable Energy Reviews*. 2017; 79:946-959.

[10]. Zhou N, Prabakaran K, Lee B, Chang SH, Harutyunyan B, Guo P, Butler MR, Timalsina A, Bedzyk MJ, Ratner MA, Vegiraju S. Metal-free tetrathienoacene sensitizers for high-performance dye-sensitized solar cells. *Journal of the American Chemical Society*. 2015; 137(13): 4414-4423.

[11]. Ooyama Y, Harima Y. Molecular designs and syntheses of organic dyes for dye-sensitized solar cells. *European Journal of Organic Chemistry*. 2009; 2009(18):2903-2934.

[12]. Bose S, Soni V, Genwa KR. Recent Advances and future prospects for dye-sensitized solar cells: a review. *Int. J. Sci. Res. Publ*. 2015; 5(4):1-9.

[13]. Giribabu L, Kanaparthi RK, Velkannan V. Molecular engineering of sensitizers for dye-sensitized solar cell applications. *The Chemical Record*. 2012; 12(3): 306-328.

[14]. Rani P. CHEMOSENSOR AND ITS APPLICATIONS

[15]. Shalini S, Balasundaraprabhu R, Kumar TS, Prabavathy N, Senthilarasu S, Prasanna S. Status and outlook of sensitizers/dyes used in dye sensitized solar cells (DSSC): a review. *International journal of energy research*. 2016; 40:1303-1320.

[16]. Susantia D, Nafi'a M, Purwaningsiha H, Fajarin R, Kusumab GE. The Preparation of Dye Sensitized Solar Cell (DSSC) from TiO_2 and Tamarillo Extract. *Procedia Chemistry*. 2014, 9, 3-10.

[17]. Yao Z, Wu H, Li Y, Wang J, Zhang J, Zhang M, et al. Dithienopicenocarbazole as the kernel module of low-energy-gap organic dyes for efficient conversion of sunlight to electricity. *Energy Environ Sci*. 2015;8(11):3192-3197.

[18]. Obotowo IN, Obot IB, Ekpe UJ. Organic sensitizers for dye-sensitized solar cell (DSSC): properties from computation, progress and future perspectives. *Journal of Molecular Structure*. 2016; 1122:80-87.

[19]. Carella A, Borbone F, Centore R. Research progress on photosensitizers for DSSC. *Frontiers in chemistry*. 2018; 6:481.

[20]. Alhamed M, Issa AS, Doubal AW. Studying of natural dyes properties as photo-sensitizer for dye sensitized solar cells (DSSC). *Journal of Electron Devices*. 2012, 16, 1370-1383.

[21]. Veikko U, Zhang X, Peng T, Cai P, Cheng G. The synthesis and characterization of dinuclear ruthenium sensitizers and their applications in photocatalytic hydrogen production. *Spectrochimica Acta Part A: Molecular and Biomolecular Spectroscopy*. 2013; 105:539-544.

[22]. Oviri OK, Ekpunobi AJ. Transmittance and Band Gap Analysis of Dye-Sensitized Solar Cell. *Research Journal of Recent Sciences*. 2013; 2(1), 25-31.

[23]. Xiaohu Z, Uahengo V, Jin M, Ping C, Tianyou P. Visible-Light-Induced Photocatalytic Hydrogen Production over Binuclear RuII–Bipyridyl Dye-Sensitized TiO2 without Noble Metal Loading. *Chemistry European journal*. 2012, 18, 12103-12111.

[24]. Kumaresan P, Vegiraju S, Ezhumalai Y, Yau SL, Kim C, Lee WH, Chen MC. Fused-thiophene based materials for organic photovoltaics and dye-sensitized solar cells. *Polymers*. 2014;6(10): 2645-2669.

[25]. Xiao Z, Chen B, Di Y, Wang H, Cheng X, Feng J. Effect of substitution position on photoelectronic properties of indolo [3, 2-b] carbazole-based metal-free organic dyes. *Solar Energy*. 2018; 173:825-833.

[26]. Hosseinzadeh E, Hadipour NL, Parsafar G. Molecular engineering of bithiazole-based organic dyes with different electron-rich linkers toward highly efficient dye-sensitized solar cells. *Journal of Photochemistry and Photobiology A: Chemistry*. 2017; 349:171-182.

[27]. Zhang X, Xu Y, Giordano F, Schreier M, Pellet N, Hu Y, et al. Molecular engineering of potent sensitizers for very efficient light harvesting in thin-film solid-state dye-sensitized solar cells. *J Am Chem Soc*. 2016;138(34):10742–10745.

[28]. Babu DD, Su R, El-Shafei A, Adhikari A. From molecular design to co-sensitization; High-performance indole-based photosensitizers for dye-sensitized solar cells. *Electrochim Acta* 2016; 198:10-21.

[29]. Huang Z-S, Hua T, Tian J, Wang L, Meier H, Cao D. Dithienopyrrolobenzotriazolebased organic dyes with high molar extinction coefficient for efficient dye-sensitized solar cells. *Dyes Pigments* 2016; 125:229–240.

[30]. Iqbal Z, Wu W-Q, Huang Z-S, Wang L, Kuang D-B, Meier H, et al. Trilateral π-conjugation extensions of phenothiazine-based dyes enhance the photovoltaic performance of the dye-sensitized solar cells. *Dyes Pigments*. 2016; 124:63–71.

[31]. Mehmood U, Rahman SU, Harrabi K, Hussein IA, Reddy BV. Recent advances in dye sensitized solar cells. *Advances in Materials Science and Engineering*. 2014; 2014.

[32]. Heo J, Oh JW, Ahn HI, Lee SB, Cho SE, Kim MR, Lee JK, Kim N. Synthesis and characterization of triphenylamine-based organic dyes for dye-sensitized solar cells. *Synthetic Metals*. 2010; 160(19-20):2143-2150.

[33]. Zhang P, Shi B, You X, Zhang Y, Lin Q, Yao H, Wei T. A highly selective and sensitive chemosensor for instant detection cyanide via different channels in aqueous solution. *Tetrahedron.* 2014 Mar 11;70(10):1889-1894.

[34]. Yu F, Cui SC, Li X, Peng Y, Yu Y, Yun K, Zhang SC, Li J, Liu JG, Hua J. Effect of anchoring groups on N-annulated perylene-based sensitizers for dye-sensitized solar cells and photocatalytic H_2 evolution. *Dyes and Pigments*. 2017, (139): 7-18.

[35]. Reichardt C. Solvatochromic dyes as solvent polarity indicators. *Chemical Reviews.* 1994; 94(8):2319-2358.

[36]. Reza HM, Javad CM, Maryam Y. Solvatochromism Effect of Different Solvents on UV-Vis Spectra of Flouresceine and its Derivatives. *Iran. J. Chem. Chem. Eng*.2008; 27(4).

[37]. Ahmed K, Auni A, Ara G, Rahman MM, Yousuf M, Mollah M, MD. Susan ABH. Solvatochromic and fluorescence spectroscopic studies on polarity of ionic liquid and ionic liquid-based binary systems. *Journal of Bangladesh Chemical Society*. 2012; 25(2), 146-158.

[38]. Masoud MS, Ali AE, Shaker MA, Ghani MA. Solvatochromic behavior of the electronic absorption spectra of some azo derivatives of amino pyridines. *Spectrochimica Acta Part A: Molecular and Biomolecular Spectroscopy*. 2004 Nov 1;60(13):3155-3159.

[39]. Tasal E, Gungor E, Gungor T. Study in the Solvent Polarity Effects on Solvatochromic Behaviour of Pomiferin. *Physical Chemistry*. 2016; 6(2): 33-38.

[40]. Kaur N, Kaur G, Fegade UA, Singh A, Sahoo SK, Kuwar AS, Singh N. Anion sensing with chemosensors having multiple N-H recognition units. TrAC. *Trends in Analytical Chemistry*. 2017 oct 1; 95:86-109.

[41]. Zhang Y, Hu W. Energy Donor Effect on the Sensing Performance for a Series of FRET-Based Two-Photon Fluorescent Hg^{2+} Probes. *Materials (Basel).*2017 feb, 10(2); 108.

[42]. Mako TL, Racicot JM, Levine M. Supramolecular luminescent sensors. *Chemical reviews*. 2018 Dec 3;119(1):322-477.

[43]. Cao J, Wang XM. An investigation of the deprotonation of hydrazone-based receptors on interaction with anion: develop a colorimetric system distinguishing cyanide from anions. *Tetrahedron*. 2013; 69(48):10267-10271.

[44]. Hu F, Cao M, Huang J, Chen Z, Wu D, Xu Z, Liu SH, Yin J. Sulfonamide and urea-based anions chemosensors. *Dyes and Pigments*. 2015; 119:108-115.

[45]. Xiao-wei H, Xiao-bo Z, Ji-yong S, Zhi-hua L, Jie-wen Z. Colorimetric sensor arrays based on chemo-responsive dyes for food odor visualization. *Trends in Food Science & Technology*. 2018 Nov 1; 81:90-107.

[46]. Patil SR, Jain PR, Sahoo SK, Redshaw C, Das D, Pradeep CP, Yu F, Chen L, Patil AA, Patil UD. A thesaurus comprising brief introduction of chemosensor for recognition of metal cations and anions. *World Journal of Pharmaceutical Research*. 2017; 6: 15, 296-340.

[47]. Lin ZH, Ou SJ, Duan CY, Zhang BG, Bai ZP. Naked-eye detection of fluoride ion in water: a remarkably selective easy-to-prepare test paper. *Chemical communications.* 2006; (6):624-626.

[48]. Lee EM, Gwon SY, Son YA, Kim SH. Properties and characteristics of squarylium-based chemosensors for Hg^{2+}. *Supramolecular Chemistry*. 2013; 25(2):61-64.

[49]. Uahengo V, Cai P, Daniel LS. A BTT-Based Colorimetric Dual Sensor for Hg (II) and Selected Anions with Molecular Logic Operations. *Advances in Chemistry*. 2016; 2016.

[50]. Kim HJ, Ko KC, Lee JH, Lee JY, Kim JS. KCN sensor: unique chromogenic and 'turn-on'fluorescent chemodosimeter: rapid response and high selectivity. *Chemical Communications*. 2011; 47(10):2886-2888.

[51]. Cui J, Lu J, Xu X, Cao K, Wang Z, Alemu G, Yuang H, Shen Y, Xu J, Cheng Y, Wang M. Organic sensitizers with pyridine ring anchoring group for p-type dye-sensitized solar cells. *The Journal of Physical Chemistry C*. 2014 Jul 31;118(30):16433-16440.